Supporting information for: Photoexcited Structural Dynamics of an Azobenzene Analog 4-Nitro-4'-Dimethylamino-Azobenzene from Femtosecond Stimulated Raman

David P. Hoffman and Richard A. Mathies*

Department of Chemistry, University of California, Berkeley, California 94720

E-mail: ramathies@berkeley.edu

Phone: (510) 642-4192. Fax: (510) 642-3599

Data Analysis

After performing the appropriate averaging of the various spectra, i.e. transient, ground and solvent, the ground state spectrum is subtracted from each transient spectra. In order to correct for any long term fluctuations in the regenerative amplifier's output, the transient spectra were normalized to the ground state spectrum using the 670 cm^{-1} line of DMSO as an internal standard. Normalizing also helps correct for the transient absorption of the Raman pump by the excited state species. This effect is non-negligible for $\lambda_{ex} = 625$ nm.

Subtracting the ground state spectrum from the transient spectra effectively removes the solvent contributions but it over corrects for the ground state contribution. Figure 1 presents representative spectra for both the 800 nm and tunable instruments, the black lines show the spectra after the

*To whom correspondence should be addressed

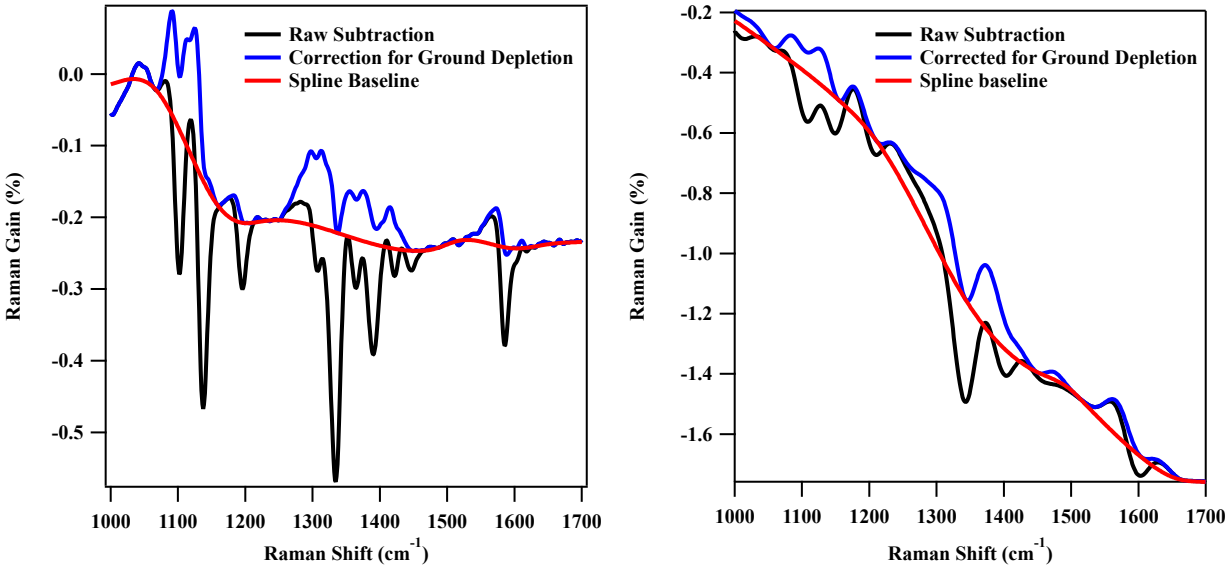

(a) Typical data from the 800 nm instrument

(b) Typical data from the tunable instrument

Figure 1: Demonstrates the main steps to extract transient FSRS spectra from the raw data. Initial subtractions are shown in black, spectra after ground state compensation are shown in blue and the baselines are shown in red.

initial subtraction. To account for the ground state depletion the pure ground state spectrum is added back to the raw subtraction until the ground state depletion is satisfactorily compensated for, shown as the blue lines in Figure 1. In order to obtain the pure ground state spectrum the solvent signals were removed by subtraction, again normalizing to the ground state spectrum using the 670 cm^{-1} mode of DMSO. Any residual baseline was then removed and the final spectrum was fit to a sum of Gaussians. This fit was used as the "pure" spectrum to avoid adding noise to the transient spectra. Finally, the baselines were removed from the ground depletion corrected transient spectra by fitting a third order spline through points chosen as the baseline and subtracting this from the spectra. The spline baseline is shown in red in Figure 1.

RINE Simulations

As mentioned in the main text, the early time transients at $\lambda_{ex} = 625$ nm are dominated by RINE. In order to test this hypothesis a simulated RINE spectrum was generated and compared to the

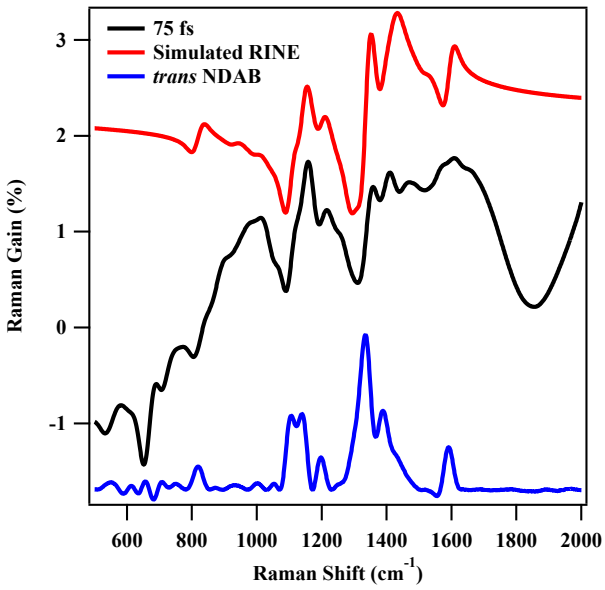

Figure 2: Simulated RINE spectra compared with the experimentally recorded 75 fs raw difference spectrum and the ground state *trans* spectrum both recorded at $\lambda_{ex} = 625$ nm. The simulated RINE spectrum (generated as described in the text) almost exactly reproduces the experimentally observed 75 fs difference spectrum. Any differences can be attributed to underlying excited state transients, this is especially visible near 1600 cm^{-1}

experimental spectra. Figure 2 presents an example comparison in which shows the experimental ground state *trans* and excited state transient at a time delay of 75 fs with the Raman pump at 625 nm. The simulated RINE spectrum almost quantitatively matches the transient spectrum especially in the CN and NN stretching regions, strongly supporting the original hypothesis. It should be noted that the transient spectrum deviates significantly from the simulated one in the NO_2 and $C-N(Me)_2$ stretching region likely due to underlying excited state resonances.

As explained by McCamant et al. [1] RINE results when the Raman pump and probe interactions produce a vibrational coherence on the ground state surface. As such the appearance of the RINE spectrum is that of dispersive peaks centered at ground state frequencies. In their derivation McCamant et al. assumed that the Raman pump had an infinite duration and found that the resulting line-shape was that of a dispersive Lorentzian. Unfortunately, the Raman pump produced by the tunable instrument has a much shorter duration which was taken into account by modeling the line-shape as a convolution of a dispersive Lorentzian with a Gaussian. With this in mind, the

ground state spectrum was analyzed and the widths, heights and center frequencies of the various vibrational resonances were extracted. Using this data, the simulated spectrum was generated by placing dispersive Lorentzians at each center frequency, scaled by the height and with a width proportional to the ground state width then the whole spectrum was convoluted with a Gaussian (FWHM of 30 cm^{-1}), this is the red line in Figure 2.

Instrument Response Functions

Figure 3 presents typical instrument response functions for both instruments.

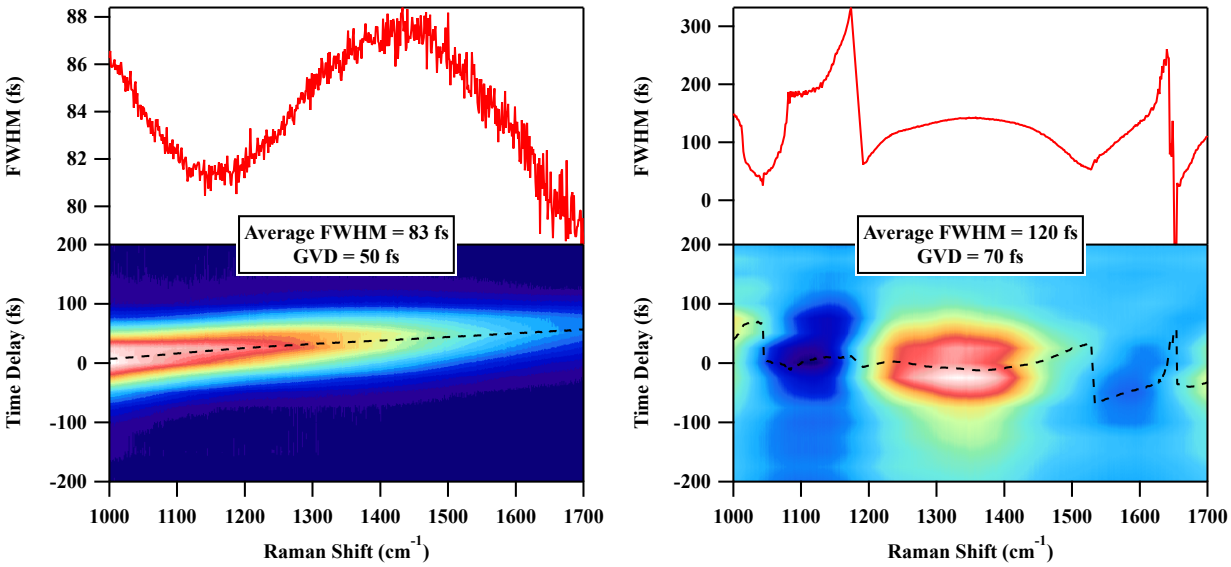

(a) $\lambda_{Apu} = 500$ nm, $\lambda_{pr} = 857 - 912$ nm **(b)** $\lambda_{Apu} = 500$ nm, $\lambda_{Rpr} = 667 - 700$ nm

Figure 3: Typical frequency resolved optical Kerr effect (OKE) cross correlation traces taken with (a) the 800 nm instrument and (b) the tunable instrument. The top trace shows how the FWHM varies with each pixel while the bottom contour shows the raw data with the position of t_0 indicated by the dotted line. Note that because of imperfections in the probe polarization and the analyzer used with the tunable instrument the OKE signal changes sign periodically leading to uncertainty in the position of t_0 and the FWHM at these pixels.

Transient Absorption

Figure 4 presents the transient absorption of *trans*-NDAB at two wavelengths. Data where recorded by modulating the actinic pump with an optical chopper (Perkin Elmer, Model 651) and amplifying the output of a photodiode (ThorLabs, DET110) with a lock-in amplifier (Stanford Research Systems, SR830).

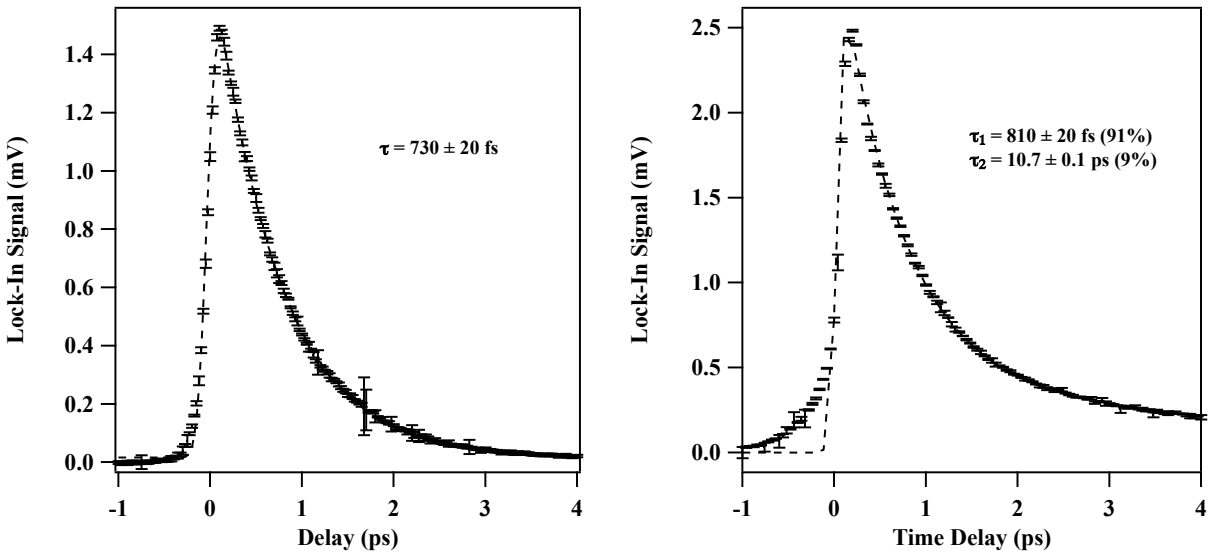

(a) Transient absorption at 790 nm

(b) Transient absorption at 625 nm

Figure 4: Transient absorption of *trans*-NDAB excited at 500 nm. (a) Show the transient absorption at 790 nm and (b) shows the transient absorption at 625 nm. Note that the trace at 625 nm is bi-exponential; 625 nm is close enough to the ground state absorption that the effects of vibrational cooling are apparent.

cis Absorption Spectrum

As mentioned in the main text the *cis* isomer of NDAB is short lived in polar solvents but has a lifetime on the order of 10-100 seconds in non-polar solvents. Complicating matters further is the fact that the absorption spectrum for the *cis* and *trans* isomers overlap substantially. Fortunately, because of the short lifetime of the *cis* isomer it was possible to record a pure *trans* spectrum after allowing the sample to dark adapt. In order to decompose the mixed spectrum, the acquisition

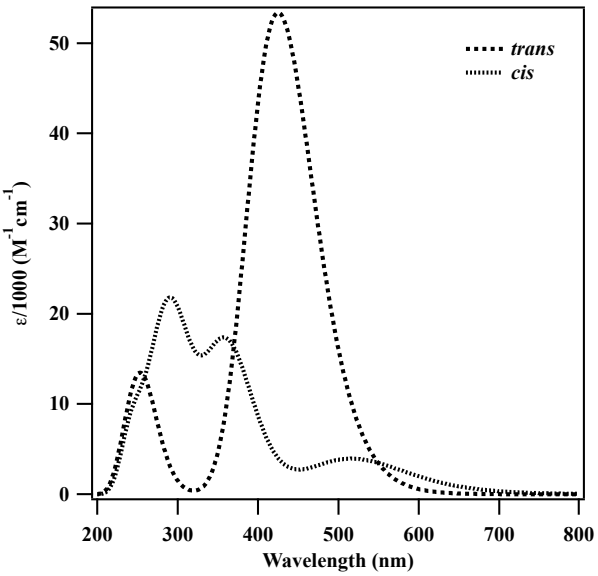

Figure 5: Calculated absorption spectra of *trans* and *cis* NDAB in CCl_4 are shown. Calculations were performed using the TD-DFT formalism with the M06-2X functional and the 6-311++g(d,p) basis set, solvent effects were included by a Polarizable Continuum Model (PCM) using the integral equation formalism variant (IEFPCM) as implemented by the Gaussian 09 software package.[2]

of which is described in the main text, the spectrum was fit to a sum of Gaussians and a scaled pure *trans* spectrum. The initial positions and intensities of the Gaussians were suggested by TD-DFT calculations on the *cis* isomer, c.f. Figure 5. The resulting *cis* spectrum was then divided by $(1 - \textit{trans}$ scale factor$)$ to obtain a properly scaled spectrum, i.e. correcting for the concentration. The results of this procedure are presented in Figure 1(a) in the main text.

Electronic Structure Calculations

In order to determine the character of the vibrational modes of NDAB, normal mode frequency calculations were performed using the DFT formalism at the B3LYP/6-311G++(d,p) level using the Gaussian 09 software package.[2] Because the calculation of IR intensities is much easier, and therefore more accurate, than calculating Raman intensities, coupled with the fact that NDAB is *not* centrosymmetric and therefore *not* subject to the mutual exclusion rule, the FTIR spectrum was used to assign the normal modes. Figure 6 presents the calculated and experimental IR spectra

demonstrating that the agreement between the theory and experiment is excellent. The normal mode characterizations based on this calculation are presented in Table 1.

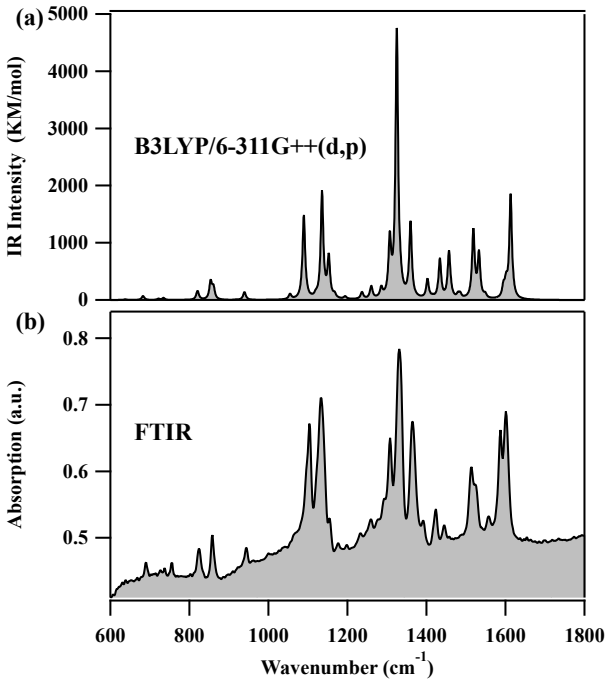

Figure 6: (a) Calculated and (b) experimental (KBr pellet, Varian, Model 3100) IR absorption spectra of NDAB. The calculated spectrum has had its frequency axis scaled by 0.978.

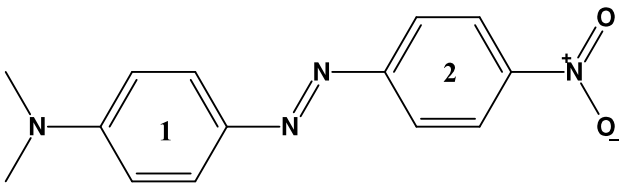

Scheme 1: *trans* 4-Nitro-4'-Dimethylaminoazobenzene (NDAB).

Table 1: A summary of the normal mode frequencies and assignments of ground state *trans*-NDAB, included are the experimentally observed frequencies using three different vibrational spectroscopies. Ring numbering refers to Scheme 1. All numbers are in cm^{-1}.

Raman $\lambda_{ex} = 497$ nm	**FSRS** $\lambda_{ex} = 790$ nm	**FTIR**	**DFT** B3LYP 6-311g++(d,p)	**Mode Character**
1105	1103	1103	1114	H rock, ring 2 breathing, CN stretch
1138	1136	1132	1161	CN stretching (both), H rock both rings
1196	1197	1198	1221	CN stretches out of phase
—	—	1259	1288	CN stretches out of phase
1307	1317	1308	1337	C(ring 1)N=N bend, H rock ring 1
1338	1336	1331	1354	N=N stretch, NO_2 symmetric bend
1367	1367	1364	1390	N=N stretch, H in phase rock ring 1
1391	1390	1393	1434	Out of phase C=C stretches (either side of ring 2) and N=N stretch
1424	1423	1423	1466	N=N stretch and C=C stretches on either side of both rings out of phase
1448	1441	1445	1490	N=N stretch and C=C stretches on either side of both rings out of phase
1588	1588	1587	1637	NO_2 asymmetric stretch C=C stretches on ring 2, N=N stretch
1604	1604	1601	1649	C−$N(Me)_2$ stretch, C=C stretches ring 1, with a little methyl deformation

References

(1) McCamant, D. W.; Kukura, P.; Mathies, R. A. *J. Phys. Chem. B* **2005**, *109*, 10449–10457.

(2) Frisch, M. J.; Trucks, G. W.; Schlegel, H. B.; Scuseria, G. E.; Robb, M. A.; Cheeseman, J. R.; Scalmani, G.; Barone, V.; Mennucci, B.; Petersson, G. A.; Nakatsuji, H.; Caricato, M.; Li, X.; Hratchian, H. P.; Izmaylov, A. F.; Bloino, J.; Zheng, G.; Sonnenberg, J. L.; Hada, M.; Ehara, M.; Toyota, K.; Fukuda, R.; Hasegawa, J.; Ishida, M.; Nakajima, T.; Honda, Y.; Kitao, O.; Nakai, H.; Vreven, T.; Montgomery, J. A., Jr.; Peralta, J. E.; Ogliaro, F.; Bearpark, M.; Heyd, J. J.; Brothers, E.; Kudin, K. N.; Staroverov, V. N.; Kobayashi, R.; Normand, J.; Raghavachari, K.; Rendell, A.; Burant, J. C.; Iyengar, S. S.; Tomasi, J.; Cossi, M.; Rega, N.; Millam, J. M.; Klene, M.; Knox, J. E.; Cross, J. B.; Bakken, V.; Adamo, C.; Jaramillo, J.; Gomperts, R.; Stratmann, R. E.; Yazyev, O.; Austin, A. J.; Cammi, R.; Pomelli, C.; Ochterski, J. W.; Martin, R. L.; Morokuma, K.; Zakrzewski, V. G.; Voth, G. A.; Salvador, P.; Dannenberg, J. J.; Dapprich, S.; Daniels, A. D.; Farkas, Ö.; Foresman, J. B.; Ortiz, J. V.; Cioslowski, J.; Fox, D. J. *Gaussian 09 Revision A.1*, Gaussian Inc. Wallingford CT 2009.